THE ASTROPHYSICAL JOURNAL, 533:454–471, 2000 April 10

ANALOGOUS EXPERIMENTS ON THE STICKINESS OF MICRON-SIZED PREPLANETARY DUST

TORSTEN POPPE, JÜRGEN BLUM[1], AND THOMAS HENNING
Astrophysical Institute and University Observatory, Friedrich-Schiller-Universität Jena, Schillergässchen 3, 07745 Jena, Germany;
poppe@astro.unit-jena.de
Received 1998 November 17; accepted 1999 November 15

ABSTRACT

In the early solar nebula, the formation of planetesimals and cometesimals is believed to be due to inelastic collisions of initially micron-sized grains. The collisions are caused by relative velocities due to size-dependent interactions with the surrounding dilute gas. The grain growth process is determined by the velocity-dependent sticking efficiency upon collisions. Therefore, we performed experiments with eight samples of micron-sized particles consisting of monodisperse silica spheres, of irregularly shaped diamond, enstatite, and silicon carbide grains, and of silicon carbide whiskers. We determined the sticking probability and the energy loss upon bouncing collisions by studying individual grain-target collisions in vacuum. We found a sticking probability higher than predicted by previous theoretical work. Grain size, roughness, and primarily grain shape, i.e., the difference of spherical versus irregular grain shape, is important for the collisional behavior, whereas the material properties are rather unimportant. Our results indicate that the preplanetary dust aggregation is more effective than previously thought.

Subject headings: accretion, accretion disks — dust, extinction — methods: laboratory — solar system: formation

1. INTRODUCTION

1.1. *Scientific Objective*

Micron-sized dust grains embedded in a dilute gas are regarded as the seeds of the planet formation in the solar nebula (Weidenschilling & Cuzzi 1993). Planetesimals and cometesimals form as a result of inelastic collisions between dust grains and because of van der Waals and other attractive surface forces, which determine physical processes such as coagulation, restructuring, compaction, and fragmentation. The low-velocity collisions, which range from a few centimeters per second to several meters per second, result from Brownian motion for the micron-sized preplanetary dust particles and from differential sedimentation, turbulence, and gas drag-induced orbital decay for millimeter-sized dust aggregates, which are believed to be fluffy grains composed of the micron-sized particles. While research on the state of the gas disk and the motion of particles therein provides information on the collision velocities and collision frequencies (see Beckwith, Henning, & Nakagawa 1998 and references therein), the collisional behavior of astrophysically relevant micron-sized grains is rather uninvestigated. In particular, the question whether or not colliding particles stick to each other is of outstanding importance for theoretical models of the dust aggregation process and will be addressed in this paper.

1.2. *Considerations for the Choice of Analogous Materials*

Mathis, Rumpl, & Nordsieck (1977) assume that interstellar grains have a size range of 0.005–1 μm for graphite and 0.025–0.25 μm for other materials. Also, in more recent work (Kim, Martin, & Hendry 1994), comparable size distributions are presented with particles of 0.1–1 μm radius dominating in mass. The dust detectors aboard the *Galileo* and *Ulysses* spacecraft have shown that local interstellar dust particles are micron sized (Grün et al. 1994). It is generally assumed that an important part of the original interstellar grains was evaporated by the accretion heat of the gas and dust disk around the forming Sun and then recondensed. This may lead to preplanetary grains having properties of recently condensed unprocessed matter. Meteoritic evidence suggests that the characteristic size of the preplanetary grains is 1 μm (Kerridge 1993; Kerridge & Chang 1987). Furthermore, the main-sequence star β Pic is surrounded by a debris dust disk whose particles have properties similar to the preplanetary dust around the young Sun and which consists of dust grains of ≈ 1 μm in size (Artymowicz 1994). The typical condensation sequence from high to low temperatures predicts that first very refractory oxides were formed and then, silicates, metals, and ices. For example, (Mg, Fe)SiO_3, (Mg, Fe)$_2SiO_4$, SiO_2, Fe, FeS, Al_2O_3, $Al_2Ca_2SiO_7$, $MgSiCa_2SiO_7$, $MgAl_2O_4$, $CaMgSi_2O_6$, and $CaAl_2Si_2O_8$ and refractory material formed of the elements C, H, O, and N are discussed to be components of the preplanetary dust in the warm regions of the inner early solar nebula (Grossman & Larimer 1974; Pollack et al. 1994; Gail 1998). In the cold outer regions, icy or ice-coated grains, consisting primarily of H_2O, are expected to dominate. Though very rare, diamond and SiC are also known to be constituents of primitive meteorites (Anders & Zinner 1993) indicating that these materials, which are, in contrast to the ones mentioned before, unmodified interstellar grains, played a role in the early solar nebula. The majority of grains important for the origin of Earth have typically in common high sublimation temperature, great hardness, high Young moduli, mainly electrically insulating material (with the important exception of iron; see Nuth et al. 1994), and intermediate or high density.

The evaporation due to the heat of the accretion disk around the forming Sun and the subsequent recondensation may lead to smooth spheroid shapes, if an even deposition of condensing molecules around a nucleus is assumed. However, irregularly shaped grains have participated in the dust aggregation as well. Irregular grains can be produced by fragmentation in high-velocity collisions or, even

[1] Present address: Naval Research Laboratory, Space Science Division, 4555 Overlook Avenue SW, Washington, DC 20375-5320; jblum@ssd5.url.navy.mil.

in needle-like shape, by crystalline condensation (Kerridge 1993). Furthermore, interstellar grains that were present in the cooler outer regions of the early solar nebula or were incorporated into the disk after the main evaporation and recondensation process may have conserved any irregular shape that they had obtained before the preplanetary dust aggregation started. The diamond and SiC grains mentioned above are examples of the latter type.

1.3. *Previous Work on Small-Particle Collisions*

Investigating the collision of particles, the treatment of spherical grains offers the easiest possibility for theoretical modeling and is an important special case both for dust coagulation and for other technical or scientific objectives. Consequently, it was studied by previous research as well as for this paper.

Hertz (1882) gave the first theoretical description of the contact mechanics of macroscopic elastic spheres under external load, providing formulae of the contact radius, the displacement, and the stress distribution within the circular contact area between two spheres.

The assumption of validity of macroscopic mechanics, elasticity, and the existence of an attractive surface force requires the existence of a capture velocity v_c below which colliding particles stick to each other and above which they bounce off. This capture velocity v_c is characteristic for collisions of small spheres. Therefore, the determination of v_c was the objective of previous investigations, mainly of engineering research motivated by the design of filters, the prevention of surface contamination, or the investigation of the behavior of particles embedded in gas flows in pipelines. The results are, e.g., important for microelectronics, chemistry, pharmacy, and nuclear industry. The previous research on the existence and on the value of a capture velocity produced a variety of different theoretical understandings, and, more important, the proposed values of the capture velocity ranged over several orders of magnitude. Important steps in this research are briefly reviewed in the following paragraphs.

Dahneke (1971) calculated the capture velocity assuming that there is an energy loss by a hysteresis effect of the elastic deformation before and after reaching the point of closest contact as well as by damping and internal friction in the deformed bulk material. If this model is applied to a silica sphere with 1 μm diameter impacting a flat silica target, the capture velocity is of the order of magnitude of 1 cm s^{-1}.

Johnson, Kendall, & Roberts (1971) developed a contact model, today often named the JKR model, which is based on Hertzian mechanics, but which was improved by introducing adhesive surface forces that increase the contact radius. The authors experimentally verified their model with centimeter-sized objects. Applied to a 1 μm silica sphere adhering to a flat silica surface and setting the surface energy of each surface to $\gamma = 0.025$ J m^{-2} (Kendall, Alford, & Birchall 1987), the separation force amounts to several 100 nN. Using a modified atomic force microscope, Heim et al. (1999) measured the separation forces between silica spheres of several diameters down to 1 μm and smooth, flat, and curved surfaces. The measurements show that, in the quasi-static case, the JKR model is applicable also for micron-sized grains.

Dahneke (1975) set up a particle-beam apparatus and performed experiments with noncharged 1.27 μm polystyrene particles impacting a polished silica target in vacuum. A vacuum environment is the realistic case for preplanetary dust coagulation and therefore important for the astrophysical relevance of the results. Although particle size and target material promise relevant results, the soft, low-density organic particle material may cause objections against an application on preplanetary dust aggregation. The particle velocity was measured by an optical time-of-flight determination. In order to describe the collisions, Dahneke introduced a kinematic value, the coefficient of restitution e, defined by

$$e = -\frac{v_i}{v_r}, \tag{1}$$

where v_i is the vertical component of the incident velocity and v_r is the vertical component of the rebound velocity. Only bouncing collisions were investigated and for the low-velocity interval, only collisions with a coefficient of restitution $e > 0.85$ were presented. To conclude on the capture velocity, Dahneke used a conservation-of-energy model consisting of two parts of energy loss upon collision. One part is determined by a coefficient of restitution e_0 being the velocity ratio directly before and after surface contact. This velocity ratio is a function only of the colliding materials, not a function of either the impact velocity or the particle size, thereby representing an increasing energy loss with increasing velocity. The other part is a constant energy value E, which is not a function of the impact velocity, thus representing the depth of a potential well created by a conservative attraction force between the surfaces. The energy balance then yields the observable coefficient of restitution

$$e = \sqrt{e_0^2 - \frac{2E}{mv_i^2}(1 - e_0^2)}, \tag{2}$$

with m being the particle mass. Dahneke (1975) introduced an e_0 that was derived from the maximum value of the measured coefficient of restitution, and he fitted his low-velocity data to this model. Setting $e = 0$, he concluded that the capture velocity of the 1.27 μm diameter polystyrene sphere on the silica target was $v_c = 1.2$ m s^{-1}. The application of the energy balance led Dahneke (1975) to choose a value of E that was 450 times higher than expected if based on known van der Waals forces. As we will see below, this obviously gave some reason to believe that such a high capture velocity v_c did not represent a typical case, but was caused by exceptional conditions, such as unusual properties of the particle materials, coatings, microasperities, or layers of water or other adsorbed molecules.

Tsai, Pui, & Liu (1990) presented a theoretical model in which the plastic deformation of surface asperities mainly determines the energy loss upon impact. The increased mechanical stress on the tips of the asperities results in plastic deformation even for low impact speeds. The surface roughness is modeled by uniformly distributed spherical asperities. These kinds of plastic deformations were also used as a possible explanation of Dahneke's (1975) results by the assumption of asperities, each having a radius of $r_{\mathrm{asp}} = 0.01$ μm and a density of $n_{\mathrm{asp}} = 260$ μm^{-2}. However, the real roughness of Dahneke's (1975) spheres is unknown, thus giving the application of this model some speculative character.

Chokshi, Tielens, & Hollenbach (1993) developed a JKR-based model of microsphere collision for astrophysical pur-

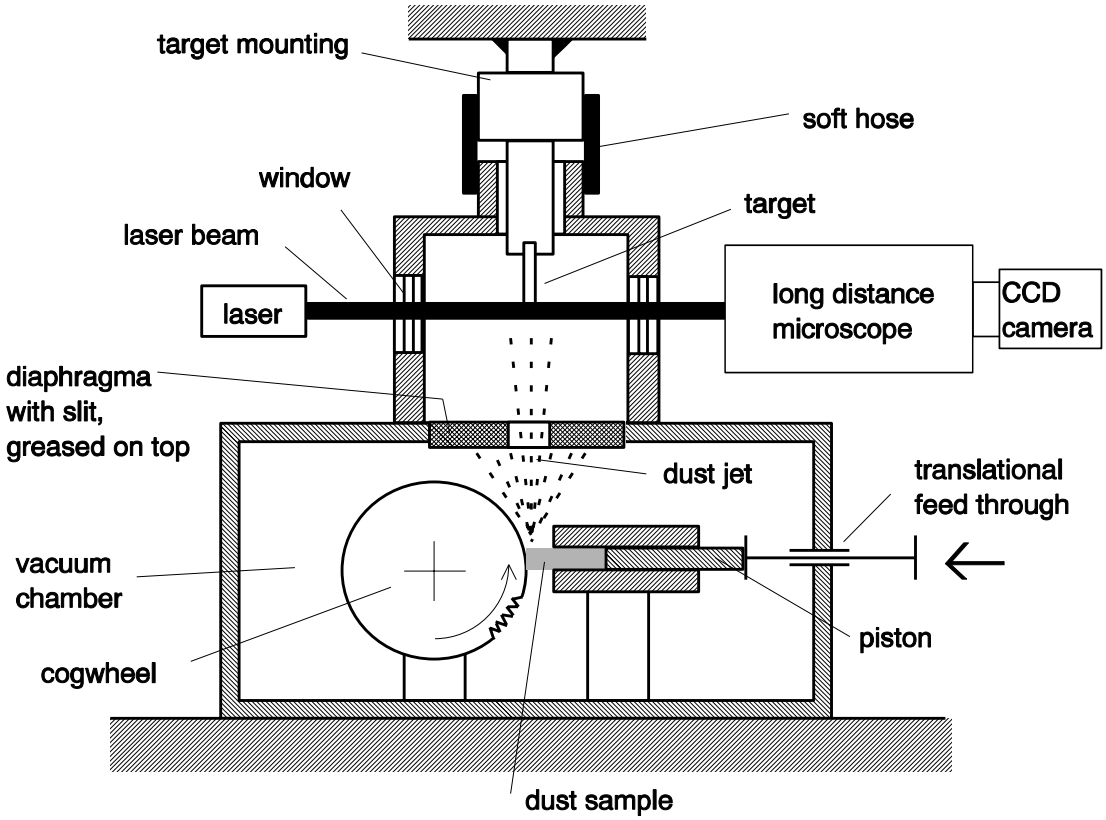

FIG. 1.—Schematical drawing of the experimental setup

poses. Apart from an energy loss due to an elastic hysteresis effect, an additional and dominating energy dissipation due to the excitation of elastic surface waves upon impact is assumed. The kinetic energy transformed into vibrational energy is mainly responsible for the kinetic energy ranges causing either sticking or bouncing. Applying the model and corrections given by Dominik & Tielens (1997) to the example of a 1 μm silica sphere colliding with a flat silica

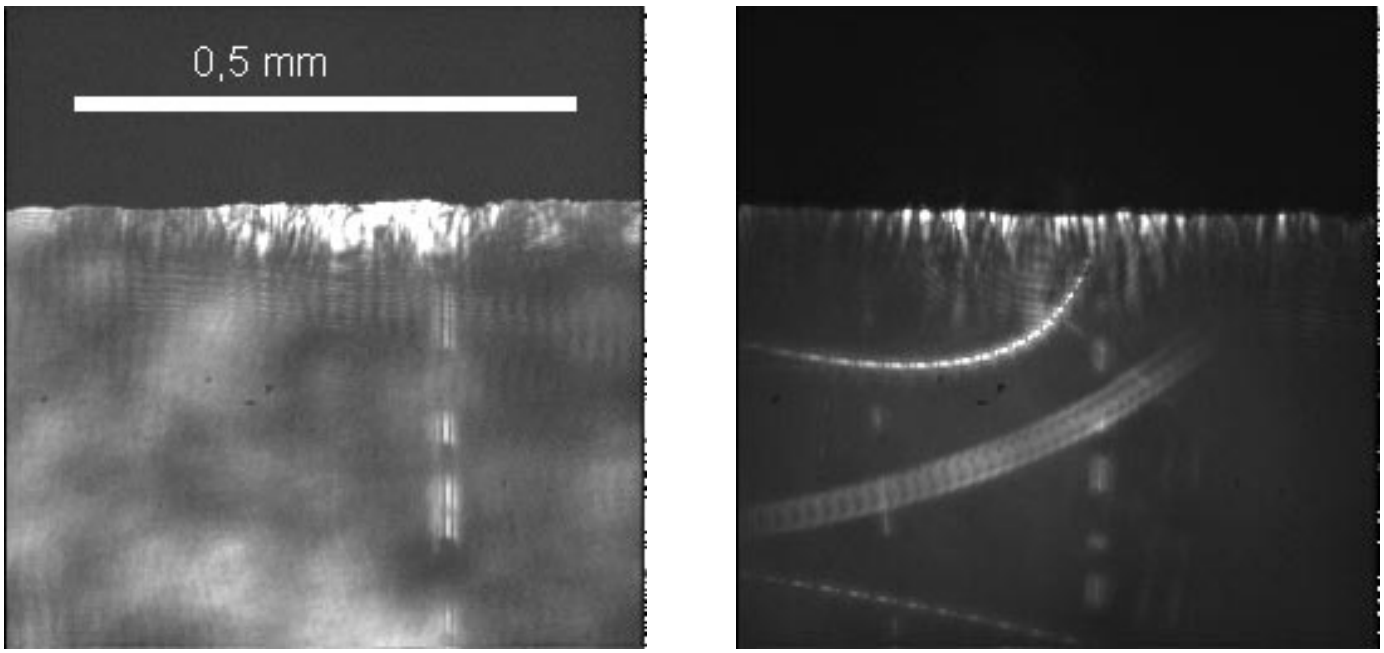

FIG. 2.—Raw images of particle trajectories that are interrupted due to the modulation of the laser illumination. This technique allows the determination of flight direction and flight velocity. Here, two silica spheres of 0.5 μm diameter impact polished silica; the left particle (impacting with 3.8 m s^{-1}) sticks, whereas the right particle (impacting with 4.7 m s^{-1}) bounces off. The target is hidden behind a diaphragm that appears as the dark upper part of the images.

surface, this leads to a capture velocity $v_c \approx 10$ cm s^{-1}. However, Chokshi et al. (1993) could not explain the results of Dahneke's (1975) experiments "within the framework" of their model.

The experimental determination of a capture velocity of single microspheres includes one more experiment carried out in vacuum for the relevant regime of large Knudsen numbers, but with comparatively large particles. Broom (1979) determined the capture velocity of particles with a diameter of 5–11 μm impacting slowly rotating wheels made of aluminum and other materials using high-speed photography. He found that the particles had a capture velocity $v_c \approx 0.1$ m s^{-1}.

John (1995) reviewed experiments that all determined the capture velocity of microspheres streaming embedded in a gas flow onto a target. The astrophysical relevance of most of these experiments suffers from the use of presumably unrealistic target and particle materials and coatings, from the generally large particle size, or from the unknown influence of the surrounding gas flows on the adhering surfaces and the real collision velocity. However, three of those experiments seem to have some relevance for astrophysical applications. The work of Wall et al. (1990) deals with a variety of target materials including silicon. These authors used quite small spheres down to 2.58 μm diameter. The microspheres consisted of ammoniumfluoresceine, which, according to § 1.2, has no important similarities to most of the materials relevant for the solar nebula. The surrounding gas pressure was reduced compared to atmospheric pressure but its actual value and thereby its influence on the collisions is unknown. Wall et al. (1990) measured the velocity of impacting and of rebounded particles by a laser Doppler technique only 10 μm away from the target and concluded on the capture velocity by fitting the measured coefficients of restitution e to an energy balance similar (but not identical; for details, see Dahneke 1995) to that one of Dahneke (1975). Wall et al. (1990) determined the capture velocity for many combinations of target material and particle size. With the smallest spheres of 2.58 μm diameter, the capture velocity was, depending on the target material, $v_c = 4$–9 m s^{-1}. Cheng & Yeh (1979) presented results of very small aerosol particles impacting stainless steel targets. They concluded that the capture velocity of 0.8 μm diameter latex spheres, the smallest particles used, on stainless steel is $v_c = 5.51$ m s^{-1}. D'Ottavio & Goren (1983) investigated the deposition efficency of solid potassium biphthalate spheres down to a diameter of 0.6 μm passing through a granular bed of pea gravel of 4 mm diameter. They concluded on a capture velocity of roughly $v_c = 7$ m s^{-1}.

Generally, authors of previous theoretical work assumed the existence of a capture velocity v_c below which particles stick and above which they bounce off. However, the experimental determination of v_c did not involve the direct observation of sticking, and it lead to values higher than those predicted by the theories.

2. EXPERIMENTAL SETUP

The setup we designed for dust-grain collision experiments is schematically shown in Figure 1. Inside the large lower part of the vacuum chamber with a pressure of $\approx$0.014 mbar, a dust jet of single micron-sized grains is created. This is done by pushing a dust powder onto the front side of a cogwheel that has a diameter of 180 mm and typically rotates with a circumference velocity of 55 m s^{-1}. The dust particles have a wide velocity distribution ranging up to the circumference velocity of the cogwheel. The particles in the dust jet seem typically to have a small number of elementary charges, which is suggested by measurements with the 0.5 μm diameter spheres, of which roughly one-quarter was uncharged. Technical details of the dust-jet generator can be found in Poppe, Blum, & Henning (1997). The particles enter the smaller upper part of the vacuum chamber through a slit in a diaphragm that is greased on its top side to avoid scattered particles.

The target mounting reaches from the top into the smaller upper part of the vacuum chamber and is connected to the vacuum chamber only by a flexible rubber tube that is used as sealing between vacuum and atmospheric pressure. This design decouples the target from vibrations of the chamber, and it allows adjustment of the target position from outside the chamber. Additionally, the target can be tilted to observe oblique impacts.

The collisions between the dust particles and the fixed target are observed by optical imaging of the particle trajectories. To achieve this, the particles are illuminated by a laser beam and observed by a long-distance microscope with attached CCD camera from outside the vacuum chamber. The focal distance of the microscope is 80 mm, and the diameter of the first lens collecting the light scattered close to the forward direction is 40 mm. The direct laser light is prevented to enter the microscope by a blind spot of 5–7 mm diameter in front of the first microscope lens. An image from an object field of (0.64 mm)^2 and a focal depth of 0.1–0.2 mm is projected onto a 256^2 pixel CCD chip leading to a resolution of 2.5 μm pixel^{-1}. The laser beam is modulated (i.e., short-off, short-on, long-off, long-on), such that the flight directions of the particles can be determined. The modulation frequency can be adjusted to allow the measurement of a broad range of velocities. From the appearance of the particle trajectories (see Fig. 2), one can easily distinguish between sticking and bouncing collisions. A major problem is the light scattered by the target, which is, due to the size of the target and due to its permanent presence on the image, much brighter than the particle. However, using a high-speed CCD camera and a microscope with a special diaphragm system, we could suppress this stray light and hence could observe the particle trajectory typically only 10–40 μm away from the point of collision; in rare cases, even the direct observation of the point of collision was possible.

3. COLLISION EXPERIMENTS WITH SILICA SPHERES

3.1. *Analogous Materials*

We used commercially available monodisperse silica spheres of 1.2 and 0.5 μm diameter and masses 1.8×10^{-15} kg and 1.3×10^{-16} kg, respectively. Examples of the particles are shown in Figure 3. From scanning electron microscope (SEM) images, we confirmed the narrow size distributions of the two samples (see Fig. 4). Rarely and especially among the larger spheres, particles can be found that appear like two spheres grown together. Among the dust sample with larger grains, there are also some very small grains detectable (see Fig. 3). The surface roughnesses were measured by atomic force microscopy with a resolution of 512^2 pixels and can be found in Table 1. It can be seen that the particles are smooth on a subnanometer scale. In any case, the measured roughnesses are smaller

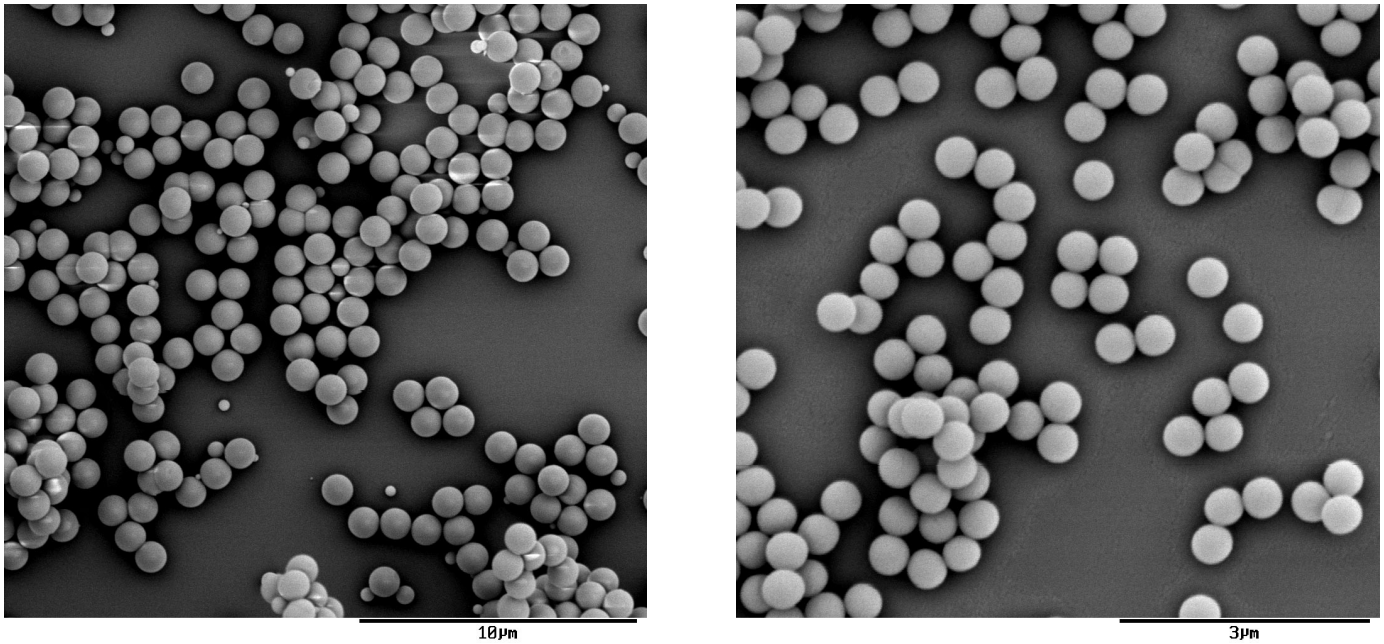

FIG. 3.—SEM pictures of the two silica dust samples

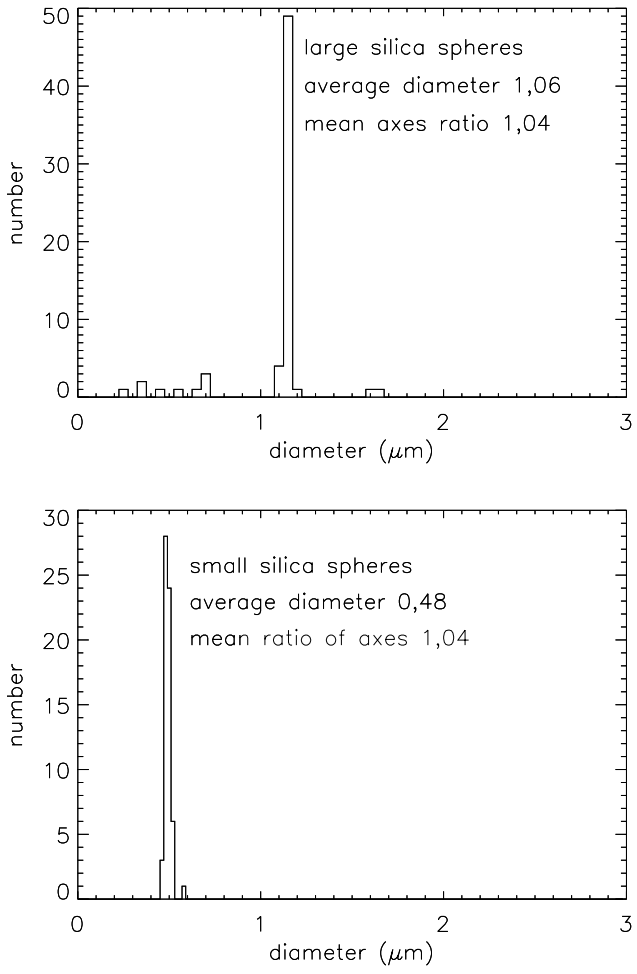

FIG. 4.—Size distributions of the two samples of silica spheres

than the indentations based on purely elastic deformation upon impact with $v_i \geq 1$ m s^{-1} (Hertz 1882). This implies that the contact occurs not only at the tips of the asperities but throughout the entire region given by the contact theory.

The particles have typical properties of preplanetary grains: (1) the micron size is characteristic for preplanetary dust; (2) the particles consist of abundant elements (Si and O) of the solids in space, and, due to the similarity to silicates, this material represents properties of an important class of preplanetary matter; and (3) the particles were produced in a supersaturated liquid where a chemical reaction deposited the SiO_2 molecules on the surface. In contrast to producing the particles from bulk material (e.g., milling), this process and the condensational growth of the preplanetary grains have the molecular deposition in common. Thus, we expect similarities concerning surface roughness and shape between preplanetary dust grains and the silica spheres used in our analogous experiments. As targets, polished flat silica surfaces and the oxidized surface of an atomically smooth silicon wafer were used (see Table 1). In order to simulate particle-particle interactions, the targets correspond to the particle materials and surfaces in many respects. The silica target and the oxidized surface of the silicon wafer consist of the same material as the impacting particles. Moreover, the silica target and the monospheres are both amorphous. A few experiments were carried out with 1.2 μm silica spheres and a silica target which both were coated with a hydrophobic layer of dimethyldimethoxysilane [$(CH_3)_2Si(OCH_3)_2$] to detect a possible influence of H_2O or other adsorbed molecule layers on the surfaces. All dust samples were kept dry under room temperature, and all flat surfaces of the silica target and the silicon wafer were cleaned with alcohol and, subsequently, dried with pressurized air.

TABLE 1

SURFACE ROUGHNESS AND SHAPE OF ANALOGOUS MATERIALS

Particle or Target	Scanned Area	δ_{rms} (nm)	σ_{rms} (degrees)	ρ_{rms} (nm)
0.5 μm silica sphere.....	50×50 nm^2	0.17	15	0.61
1.2 μm silica sphere.....	50×50 nm^2	0.56	22	0.48
Silica target.....	2×2 μm^2	1.03	1.8	373
	50×50 nm^2	0.29	18	0.55
Silicon wafer	2×2 μm^2	0.57	0.6	831
	50×50 nm^2	0.14	6.1	1.43

NOTE.—The quantity δ_{rms} is the root mean square deviation from the average surface profile, σ_{rms} is the mean surface inclination, and ρ_{rms} denotes the mean radius of surface curvature.

3.2. *Results*

For a total of 858 impacts between spherical SiO_2 particles and flat targets, we determined the velocity of the impacting grains and observed whether there was a trajectory of a rebounding particle on the images of the type shown in Figure 2. Frequently, curved particle trajectories were observed that showed a particle bouncing off and then returning to the target. This effect can be explained by collisional grain charging and a subsequent electrostatic attraction by the collisionally charged target. In contrast to surface forces, the electrostatic interaction is a long-range effect that leads to an unambiguous detection of any rebounding particle. In this context, we regard such collisions as bouncing collisions since a mechanical rebound occurs that could always be detected. However, those particles would finally stick to the target, so collisional grain charging is also important with respect to sticking. We will present experiments on collisional particle charging in a separate paper (Poppe et al. 2000).

Figure 5 presents an overview of all observed collisions indicating the particle diameter, the impact velocity, the type of particles, the collisional condition, and whether sticking (ticks above the horizontal lines in Fig. 5) or rebound (ticks below the horizontal lines in Fig. 5) were observed. For the 1.2 μm diameter spheres, the hydrophobic silane coating did not change the collisional behavior as well as the existence and the numerical value of the capture velocity significantly. Therefore, we exclude the collisions observed with the hydrophobic surfaces from the database treated from here on.

For the determination of the sticking probability and the capture limit, the collisions were sorted according to their

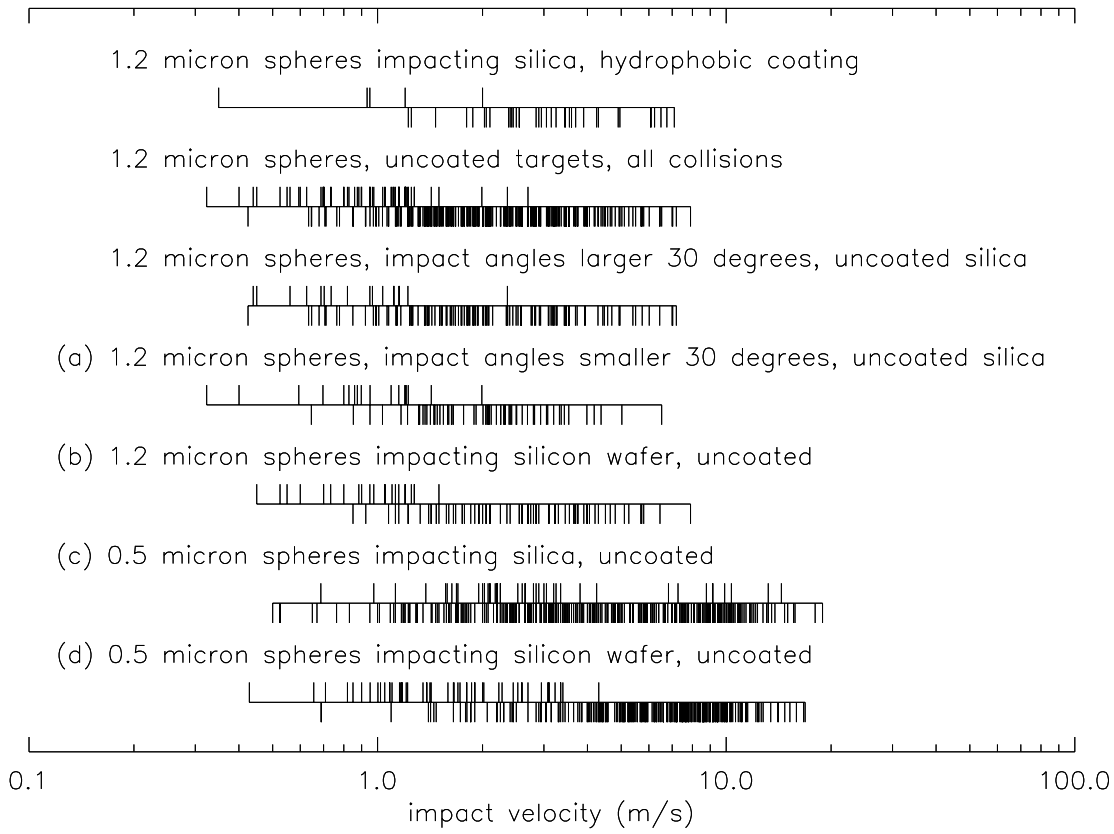

FIG. 5.—Experimental conditions and impact velocities for all observed collisions of the silica spheres. A tick to the top indicates sticking; a tick to the bottom, bouncing. Sizes are diameters.

impact velocity. For each collision velocity, the sticking probability was calculated by sliding averaging in groups. The groups consisted of 11 collision events for the smallest and largest velocities, respectively and of up to 71 collision events for the intermediate velocities, thus accounting for the uneven velocity distribution of the impacts. The upper and lower standard deviations ($\pm 1\ \sigma$) for the sticking probability are presented in Figure 6. Since this procedure cannot be applied to the slowest and to the fastest collisions, the sticking probability among the 11 slowest and the 11 fastest collisions is separately given as a constant value in the corresponding velocity interval; additionally, the outcomes of theses collisions are marked according to the way used in Figure 5. For our measurements, we define the capture velocity v_c as the velocity where the $\pm 1\ \sigma$ limits of the sticking probability are 0.5. Such a definition results in a physically meaningful quantity only if the sticking probability behaves similar to a step function. For the 1.2 μm diameter spheres, we find $v_c = 1.1$–$1.3\ \mathrm{m\ s^{-1}}$ on both targets, and for the 0.5 μm diameter spheres impacting the silicon wafer, the capture velocity is $v_c = 1.5$–$2.3\ \mathrm{m\ s^{-1}}$. In contrast to these impacts, the collisions between the 0.5 μm silica spheres and the silica target show a relatively flat sticking probability with an average value of 0.13 and a statistically significant local maximum at $1.9\ \mathrm{m\ s^{-1}}$ collision velocity. In this case, it makes no sense to speak of a capture velocity.

For the 1.2 μm silica spheres, we have also performed collision experiments with tilted silica targets. Figure 7*a* shows the data points on the collisional outcome plotted over the absolute value of the impact velocity (not over the vertical component of the impact velocity as in all other figures). The experiments covered impact angles from 0° to 60°. It can be seen that, within statistical uncertainties, the velocity limit between sticking and bouncing is no function of the impact angle for impact angles smaller than 60°. The low number of sticking collisions for the very high impact angles of 50°–60° is an artifact caused by limitations of the particle trajectory observation close to the target. As we will see below, the rebound angle may differ significantly from the impact angle, which may lead to a hidden trajectory in case of rebound. We only included data of sticking collisions into the diagram when it was certain that there was no hidden rebounding trajectory. This, of course, results in a selection effect overrepresenting rebounding collisions. The assumption of an impact angle-independent capture velocity is supported by the fact that the lower velocity limit for which bouncing collisions were observed is also independent of the impact angle.

Figure 7*b* shows the impact angles and the corresponding rebound angles of the 1.2 μm particles impacting polished silica. Due to the trajectory imaging method, the indicated impact and rebound angles are two-dimensional projec-

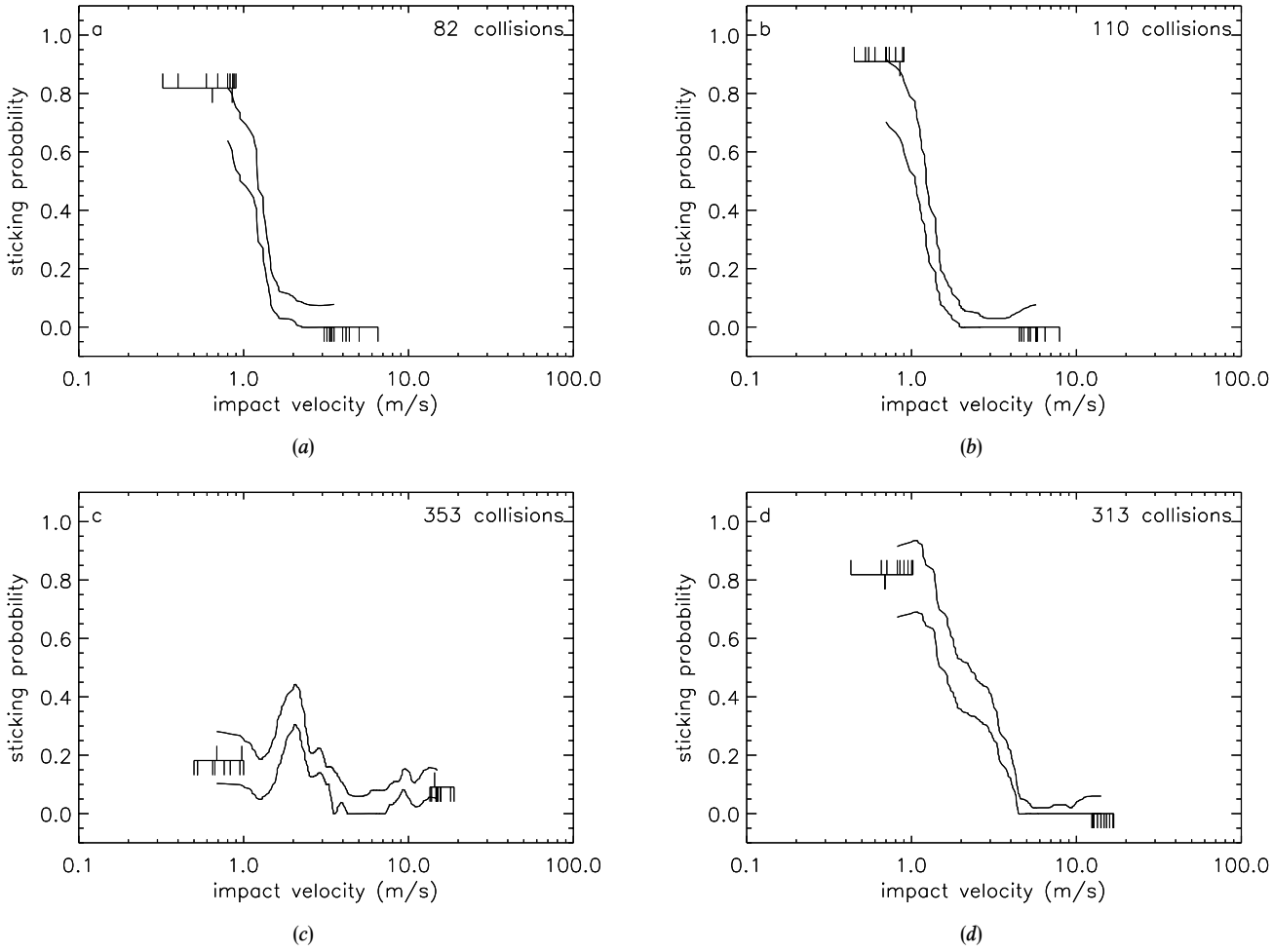

FIG. 6.—Sticking probability as a function of impact velocity for silica spheres of (*a*) 1.2 μm diameter impacting polished silica, (*b*) 1.2 μm diameter impacting a silicon wafer, (*c*) 0.5 μm diameter impacting polished silica, and (*d*) 0.5 μm diameter impacting the silicon wafer. The two solid lines in each plot denote the upper and lower 1 σ uncertainty limit for the sticking probability. Additionally for the slowest and fastest collisions, the average values of the sticking probability is shown as a constant value with each single collision marked in the way introduced in Fig. 5.

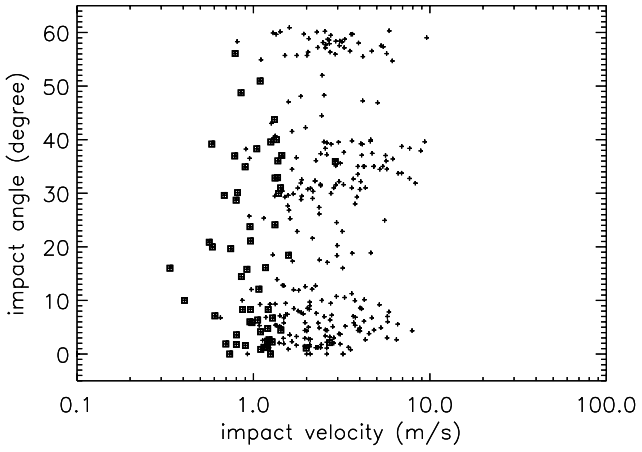

(*a*)

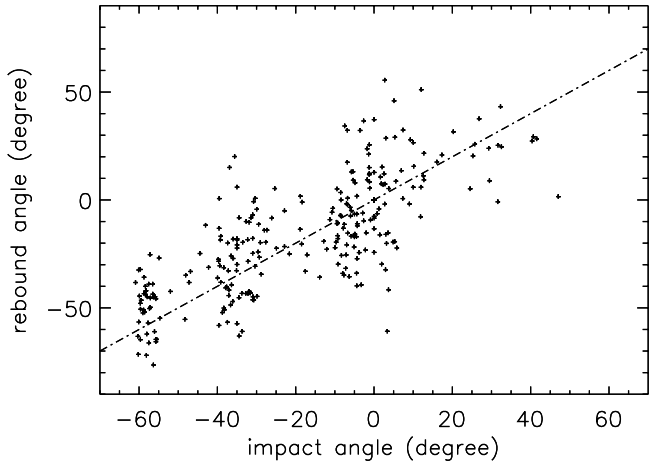

(*b*)

FIG. 7.—(*a*) Absolute value (not vertical component as in other figures) of impact velocity and impact angle for sticking (*squares*) and bouncing collisions (*crosses*) of 1.2 μm silica spheres. (*b*) The impact angle and two-dimensional projection of the rebound angle observed with silica spheres of 1.2 μm diameter.

tions. Since the particles reach the target through a small slit, the difference between projected and true impact angles should be rather low, whereas this difference may be larger for the rebound angles. The data in Figure 7*b* indicate that the deviations from specular reflection are rather substantial. Impact and (projected) rebound angle can differ by up to 30°. Assuming an undetectable velocity component toward or away from the observer with the same average value as the observable component, the change in flight direction is even larger. This deviation from specular reflection cannot be explained by the typical inclination of the surface roughness that was presented in Figure 1. Instead, the change of flight direction can obviously only be explained by a particle rotation with the rotational and translational energy of the impacting particle being typically of the same order of magnitude.

According to equation (1), the coefficient of restitution is shown in Figure 8. Individual data points vary strongly, and the mean coefficient of restitution is typically smaller than those of former experiments (Dahneke 1975; Wall et al. 1990). For impact velocities between 1 and 10 m s^{-1}, the kinetic energy is typically reduced to one-half for the 1.2 μm and to one-quarter for the 0.5 μm diameter silica spheres; for impact velocities exceeding 10 m s^{-1}, the bouncing collisions reduced the kinetic energy by more than one order of magnitude. For the 0.5 μm silica spheres, the average coefficient of restitution is lower, and the variation is slightly smaller for impacts on the silicon wafer as compared to the polished silica target. In rare cases, a coefficient of restitution $e > 1$ was found, which means that the vertical component of the incident velocity was smaller than the vertical component of the rebound velocity. This can be explained by a transformation of rotational energy into translational energy in the case of oblique impacts, since it is probable that the particles rotate. In the case of normal or near-normal impacts on flat surfaces, no plausible mechanism for the transformation of rotational into translational energy is known to the authors. The following effects or errors due to the experimental method are excluded or regarded as extremely unlikely:

1. The probability of the trajectories of the approaching and of the reflected grain belonging to different particles is practically zero. Furthermore, if this effect was still the cause, coefficients of restitution exceeding unity would be equally distributed in the entire velocity interval. Instead, they occur only at velocities where high coefficients of restitution typically appear.

2. The approaching trajectory could be the two-dimensional projection of an oblique impact, which appears, due to projection effects, as a normal impact. However, the typical length of the particle trajectories is 400 μm, and the depth of focus restricts the possible impact angle to less than 25°. Even such oblique trajectories are very unlikely since the greased top side of the entrance aperture between the large lower and the small upper part of the vacuum chamber prevents particles to bounce off from there.

3. More mass could approach the target than is rebounded corresponding to a small aggregate that is fragmented into exactly one rebounded and one sticking part. If this was the case, one would expect that also collisions of small aggregates fragmenting into more than one bouncing part should occur, but this was never observed. It is known that the dust jet consists of single particles and large aggregates consisting of 10,000 particles, whereas small aggregates were never found (Poppe et al. 1997). The large aggregates can be, and were, resolved and distinguished from the single particles and they, in fact, fragment into many parts. From this, we conclude that only single-particle collisions were observed.

4. The kinetic energy of the particle is increased by vibrations of the target. However, the low resonance frequency of the target mounting and the fact that no sufficient target motion could be seen by high-speed imaging allows us to exclude this possibility.

We will discuss possible physical effects responsible for the occurrence of $e > 1$ in § 3.3.

3.3. *Discussion*

The collisional behavior of silica spheres and smooth targets can reasonably be characterized by a capture velocity v_c, defined as the impact velocity at which the sticking probability is 0.5. For the experiments described in the previous section, we found the existence of such a threshold velocity for collisions between 1.2 μm SiO_2 spheres and polished silica as well as a silicon target and for collisions

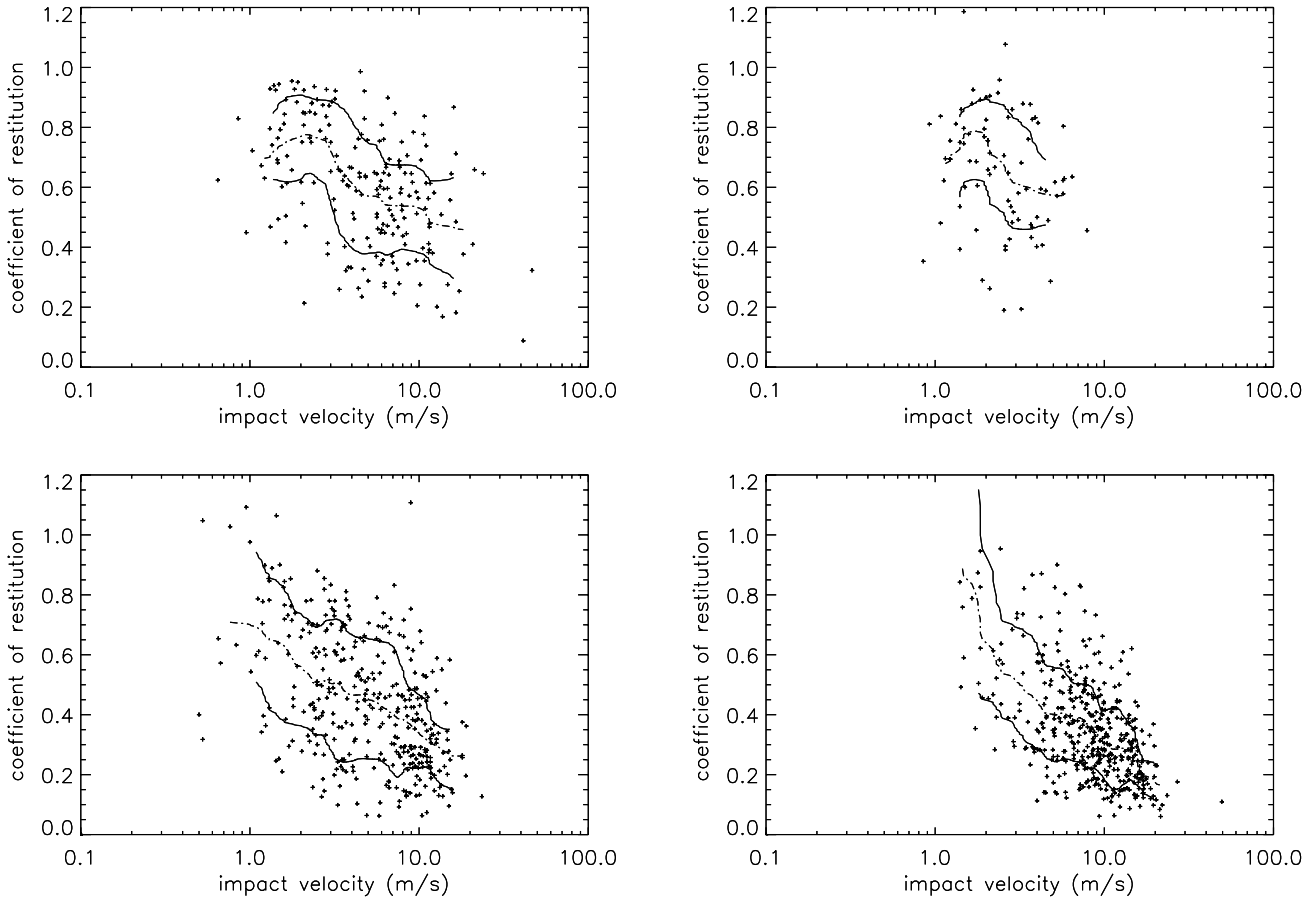

FIG. 8.—Coefficients of restitution as a function of impact velocity for silica spheres of (*upper left-hand panel*) 1.2 μm diameter impacting polished silica, (*upper right-hand panel*) 1.2 μm diameter impacting a silicon wafer, (*lower left-hand panel*) 0.5 μm diameter impacting polished silica, and (*lower right-hand panel*) 0.5 μm diameter impacting the silicon wafer. The upper and lower standard deviations of the data points (*solid lines*) and the average value (*dashed lines*) are shown. Not shown in the lower right-hand diagram are the highest coefficients of restitution $e = 1.4$ and $e = 1.5$ ever observed. Some diagrams contain additional observations of collisions with higher velocities compared to the diagrams in Fig. 6.

between 0.5 μm SiO_2 spheres and a silicon wafer. The capture velocities are 2 orders of magnitude higher than could be explained by the assumption of an elastic hysteresis effect with measured surface energies as done by Dahneke (1971) and more than 1 order of magnitude higher than predictions by the model of Chokshi et al. (1993), who assumed an additional energy dissipation due to the excitation of surface vibrations upon impact.

In the following, we exclude increased surface forces, plastic deformation of microasperities, and electrostatic effects as being the major energy dissipation mechanisms that are responsible for the higher capture velocity.

Heim et al. (1999) measured the pull-off forces between the same silicon wafer and the same type of silica spheres as used here. For particle diameters between 1 and 5 μm, they found a linear relation between the pull-off force (ranging from 50 to 250 nN) and the grain size in agreement with the predictions by the JKR model. As a result, Heim et al. (1999) deduced a specific surface energy of $\gamma = 0.019$ J m^{-2}, which corresponds to the earlier value of $\gamma = 0.025$ J m^{-2} by Kendall et al. (1987). In addition, an increased surface energy due to, e.g., adsorbed H_2O layers is not the cause of the high capture velocity as indicated by the fact that the collision experiments using particles coated with a hydrophobic layer of silane showed no significant difference from those with noncoated surfaces. Thus, an increased "stickiness" of the surfaces in contact does not exist.

If the plastic deformation of surface asperities as proposed by Tsai et al. (1990) were the dominating energy-loss channel, voluminous surface asperities would be correlated to high capture velocities. However, this is obviously not true for both types of spherical particles. With the 1.2 μm silica spheres, no difference in the capture velocity was found between the smooth silica target and the even smoother silicon-wafer target. With the 0.5 μm silica spheres, the smoother silica wafer captured the particles more efficiently than the rougher silica target within the observational range of velocities. Hence, plastic deformation of surface asperities cannot account for the capture velocities observed.

Concerning electrostatic effects possibly masking a low capture velocity, we argue based on results of Poppe et al. (2000) and Poppe (1998). Generally, electrostatic charging is only important for velocities exceeding 10 m s^{-1}. Nevertheless, charging rarely occurs at lower velocities. Based on our measurements of collisional charging, we take a maximum possible charge transfer with uniform sign (although the sign is not uniform but there is a dominating negative sign) for impacts at the capture velocity. This maximum charge transfer is $n = 1$ and $n = 10$, elementary charges for the 0.5 and 1.2 μm silica spheres, respectively. In addition, it was found that the surface charge density on the target was $Q_A = 10^{-5}$ C m^{-2}. For the potential case that the impacting particles are reflected off the surface but reattracted to

the target by electrostatic fields within the unobservable range of $s \leq 40$ μm, we can formulate the maximum possible energy loss. Charge separation in a collision leads to a buildup of an electrostatic field in which the rebounding particle is traveling along the field lines. This leads to a maximum energy loss of $E_1 = (nq)^2/(4\pi\epsilon_0 z_0)$. Here, q, ϵ_0, and $z_0 = 0.4$ nm are the elementary charge, the dielectric constant, and the equilibrium distance of the two surfaces in contact. In addition, the surface charge on the target attracts the oppositely charged rebounding particle and leads to a further energy loss of $E_2 = (1/\epsilon_0) \times (Q_A nqs)$. The maximum total energy loss is, thus, $E_{\rm tot} = E_1 + E_2$. This compares to the minimum kinetic energy observed for rebounding particles of $E_r = (1/2) \times [m(ev_c)^2]$. In Table 2, we list these energies for both types of particles. Although charge transfer nq, coefficient of restitution e, and spatial extent s of the hidden volume were chosen to the extreme values to support an electrostatically caused effect that could be mistaken as a capture velocity, the corresponding energy loss $E_{\rm tot}$ cannot prevent the particle from entering the observed volume. Thus, we also exclude electrostatic effects as the cause of observing a capture velocity exceeding 1 m s^{-1}.

Having excluded surface effects (roughness and charging), we conclude that the high capture velocity must mainly be determined by an effective and hitherto underestimated and unknown dissipation of energy in the bulk material of microscopic dust grains.

Since our target materials and particle sizes are very similar to the parameters in Dahneke's (1975) collision experiments, his calculation of a capture velocity based on measurements of the coefficient of restitution e of bouncing collisions and our new measurements confirm each other and suggest that a capture velocity of the order of m s^{-1} for micron-sized grains seems to be typical.

Using a capture velocity $v_c = 1.2$ m s^{-1} and $v_c = 1.9$ m s^{-1} for the two sphere diameters of $d = 1.2$ μm and $d = 0.5$ μm, respectively, and assuming that the size function is a power law, we propose

$$v_c \propto d^{-0.53} \tag{3}$$

as a scaling law.

John (1995) reports that the capture velocity decreases with increasing impact angle if the normal component of impact velocity is regarded. Our measurements confirm this for angles between 0° and 60° (see Figs. 5 and 7) and suggest that the absolute value of the capture velocity is constant over the entire range of our collision angles. As we have covered all impact angles between 0° and 60°, our results are valid for one half of all random collisions between spherical particles.

Generally, the coefficient of restitution is so low that the particles lose the majority of their kinetic energy. For collisions exceeding 10 m s^{-1}, the kinetic energy is typically reduced by one order of magnitude.

The fact of coefficients of restitution $e > 1$ occasionally occurring may be explained with particle rotation for oblique impacts, but there is no plausible mechanism based purely on the validity of macroscopic mechanics for normal impacts on smooth surfaces that could explain the energy transfer from rotational to translational energy. Here, we list three hypotheses to explain the singular occurrence of collisions with $e > 1$ and we judge their plausibility:

1. Electrostatic effects could be responsible for $e > 1$. Again, we base our considerations on results of Poppe et al. (2000). Generally, electrostatic charge transfer is of minor importance for the low-velocity regime in which $e > 1$ was observed. If the particles had charged themselves with the same sign as the precharged target (which is rare but not impossible) the particles would have been repelled by the target within the observed volume. However, the trajectories of these particles indicated no acceleration as would be necessary if this effect was the cause for $e > 1$. Also the idea that the particle could impact onto an electrically highly charged spot and could then acquire a part of the charge whose repulsive force could cause the high rebound velocity appears, based on the experimental evidence, highly implausible because there is no evidence for charge sharing (i.e. excess surface charge flowing from the highly charged to the less-, non-, or oppositely charged insulating surface in touch) and because one counterexample where charge transfer can definitely not account for $e > 1$ was found.

2. The particle could not be spherical and rotate such that rotational energy could be transformed into translational degrees of freedom. Rarely, nonspherical particles could be found in our dust samples that look like two spheres grown together. These grains in principle allow a transformation of rotational energy into translational also for normal impacts. Rotational direction, angular velocity, and impact angle must act together and the typical (but not the only possible) effect of an irregular shape rather seems to be a high translational energy loss than an energy gain as we will show in § 4.3 of this paper. As our 1.2 μm sample contains more of the binary particles, one would expect that $e > 1$ events play a more important role for these than for the smaller spheres. Instead, observations with $e > 1$ are more frequent and have higher values of e for the 0.5 μm dust grains that are of much better uniformity than the larger ones. Therefore, we regard the above-mentioned hypothesis as unlikely though not impossible.

3. Potential energy may be stored in a particle deformation and released upon impact because the dust sample was mechanically deagglomerated by the cogwheel dust-jet generator and may have undergone strong mechanical stress and deformation not just at the point of contact but possibly in the bulk of the whole particle. It could be considered that, with very small deformation scales, δ, the elastic redeformation may partially be staunched or inhibited and

TABLE 2

MAXIMUM ENERGY LOSS $E_{\rm tot}$ INSIDE THE UNOBSERVABLE VOLUME CLOSE TO THE TARGET AND MINIMUM REBOUND ENERGY E_r RESULTING FROM NONSTICKING IMPACT AT CAPTURE VELOCITY

	PARTICLE DIAMETER	
ENERGY	1.2 μm (J)	0.5 μm (J)
E_1	5.8×10^{-17}	5.8×10^{-19}
E_2	7.0×10^{-17}	7.0×10^{-18}
$E_{\rm tot}$	1.3×10^{-16}	7.6×10^{-18}
E_r	3.2×10^{-16}	3.8×10^{-17}

NOTE.—E_1 and E_2 specify the contributions to $E_{\rm tot}$ due to charge separation and escape in a homogeneous electrical field.

is later initiated upon impact. The existence of a release of potential energy would be in agreement with the fact that it could also account for the strong variation of the coefficients of restitution e observed with especially the small, 0.5 μm diameter spheres.

However, there is no proof for any of these hypotheses. Hence, the reason for the very rare case $e > 1$ remains unclear.

Dahneke (1975) and Wall et al. (1990) found in their experiments that the coefficient of restitution decreases toward the capture velocity, which allowed them to deduce the capture threshold from the coefficients of restitution by applying an energy balance equation. For the larger silica spheres, we found a similar behavior for the coefficient of restitution. However, for the application of an energy balance calculation, the scatter in our data seems to be too strong. For the smaller spheres, not only the scatter is larger but there is also no decrease of the coefficient of restitution toward the capture velocity. We consider that these variations in the values of the coefficient of restitution are due to the extremely small contact areas and deformations, since, compared to previous experimental research (Dahneke 1975; Broom 1979; D'Ottavio & Goren 1983; Wang & John 1988; Esmen et al. 1978; Cheng & Yeh 1979; Rogers & Reed 1984) our experiments involved smaller and harder particles leading to the smallest contact radii ever investigated.

Small contact radii, and, hence, the occurrence of statistical effects, can explain why we found a transition range, no capture velocity on polished silica for the small grains, and a strong variation of the coefficient of restitution. This is supported by the fact that the above-mentioned effects occur or are more relevant for the smaller particles. The comparison between small and large SiO_2 particles impacting the silicon wafer shows that the transition range between sticking and rebound increases relatively and absolutely with decreasing particle size. For the 0.5 μm particles, the transition range reaches half the value of the capture velocity itself. However, for the 0.5 μm SiO_2 spheres impacting the slightly rougher silica target, a capture velocity could not be found. Instead, a relatively constant sticking probability of 0.13 was detected for the impact velocity range of 0.5–10 m s^{-1}. The sticking probability seems to be sensitive to influences of tiny surface roughnesses which prevent a close surface contact and thus reduce the effective contact area. In this context, surface roughnesses have the opposite effect on the sticking probability compared to the theory of Tsai et al. (1990), who argued that small asperities increase the capture velocity and the sticking probability.

4. COLLISION EXPERIMENTS WITH IRREGULARLY SHAPED GRAINS

In the previous sections we have seen that the collisional behavior of spherical particles can be characterized by a sticking threshold. For collisions between very small grains, deviations from this idealized picture were observed. To expand the empirical information on the collisional behavior of nonspherical particles, we also performed impact experiments with irregularly shaped grains of various sizes and materials.

4.1. *Analogous Materials*

SEM images of the irregularly shaped particles are shown in Figure 9. Figure 10 presents the size distributions that were derived from these images. The grain diameter derived for the irregularly shaped particles is the average of long and short axes presented in Figure 9. We used irregularly shaped diamond grains of two size distributions, namely a small sample of 0.1–0.4 μm (average 0.14 μm) (Figs. 9*e* and 10*e*) and a large sample of 1.3–1.9 μm (average 1.5 μm) diameter (Figs. 9*f* and 10*f*). The diamond grains were artificially produced for industrial purposes. We also used enstatite grains ($MgSiO_3$) of 0.2–1.0 μm (average 0.54 μm) diameter (Figs. 9*g* and 10*g*), produced from amorphous bulk material that was milled into grains and sedimented in order to obtain a fraction of small grains. Details of this process can be found in Dorschner et al. (1995). Furthermore, we used three different silicon carbide dust samples. The small silicon carbide grains have a diameter ranging from 0.2 to 1.0 μm and an average diameter of 0.37 μm (Figs. 9*h* and 10*h*). The larger grains have a diameter ranging from 0.2 to 1.5 μm with an average of 0.64 μm (Figs. 9*i* and 10*i*). The third silicon carbide dust sample consists of whiskers with up to 90 μm length (Fig. 9*j*). The target in all experiments was polished silica as described in § 3.1.

4.2. *Results*

Figure 11 gives an overview of sticking or bouncing for all collisions of irregularly shaped grains observed. The sticking probability was statistically determined in the way described in § 3.2 for the silica spheres. Figure 12 presents the 1 σ limits of the sticking probability as a function of impact velocity. The irregularly shaped grains impacting the polished silica target behaved in a different way than the silica spheres, since there is no clear capture velocity in the velocity range observed. Instead, some types of grains can better be described with a constant sticking probability in the entire velocity range of investigation. However, a capture velocity below which the sticking probability exceeds 0.5 and above which it is smaller 0.5 can always be defined and is justified in a few cases (f, g, i). Table 3 shows the capture velocities and (mean) sticking probabilities obtained. For the sake of comparison, the results of the silica sphere collisions presented in § 3 are also given. The silicon carbide whiskers were by far the largest grains used in the collision experiments. The lengths of the whiskers could be resolved on the microscopic images and thus are shown for each individual collision on the lower right in Figure 12. The sticking probability for the collisions between SiC whiskers and polished silica targets is rather a function of particle length than of impact velocity because there were more sticking collisions observed for the short whiskers than for the longer ones, whereas the sticking probability is no obvious function of impact velocity.

The determination of a coefficient of restitution was impossible for most collisions because the rebound velocity was too small to be resolved by the laser modulation periods on the CCD images. From this, we can estimate that the irregularly shaped grains impacting a flat surface normally have a coefficient of restitution $e < 0.1$.

4.3. *Discussion*

We have seen in the previous sections that the most important effect is an increase of the capture velocity and the sticking probability in the case of irregularly shaped grains. If a capture velocity is used for the description of collisional behavior, it is many times higher for the irregular

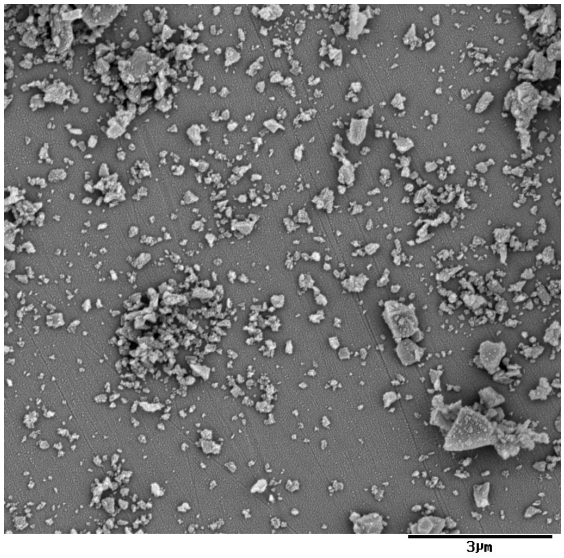

(e)

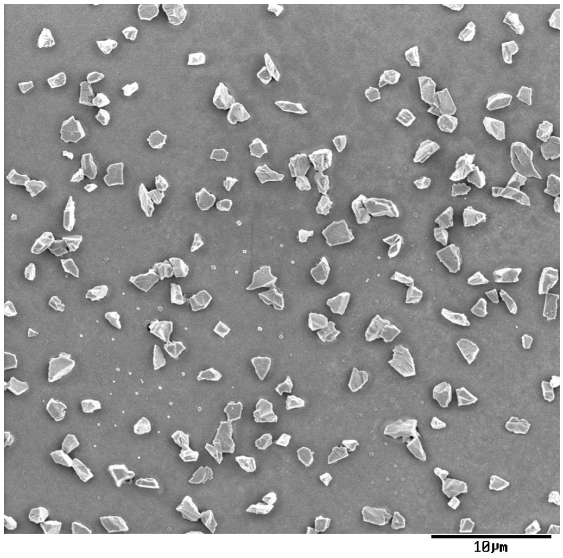

(f)

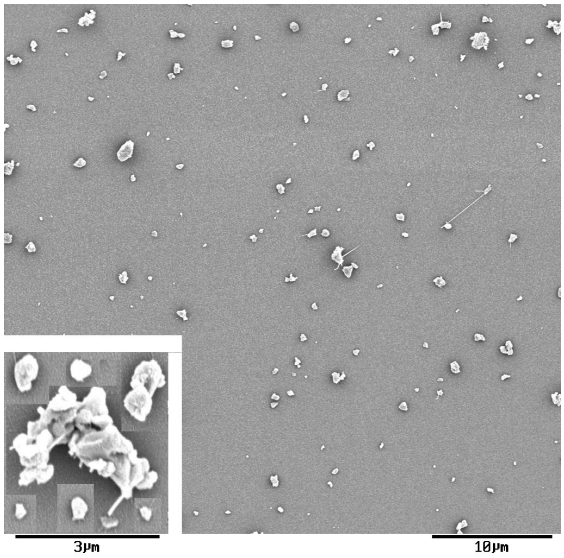

(g)

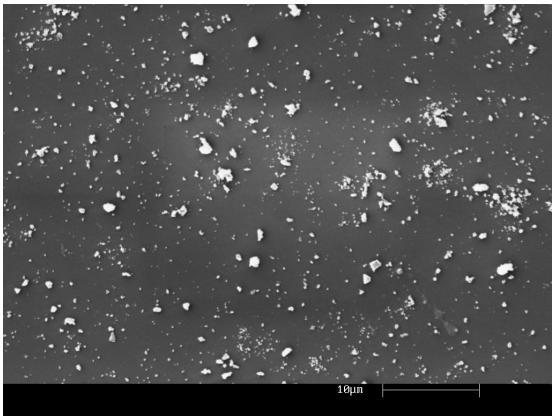

(h)

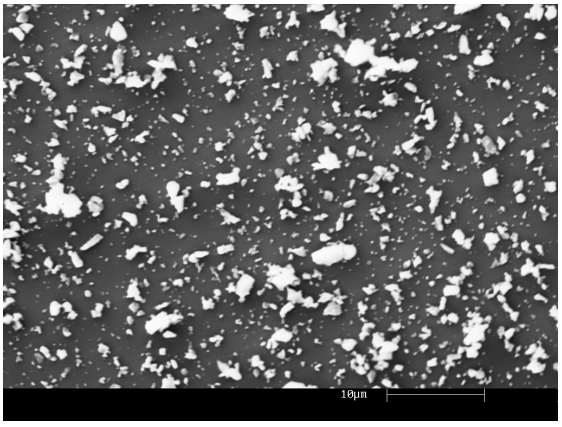

(i)

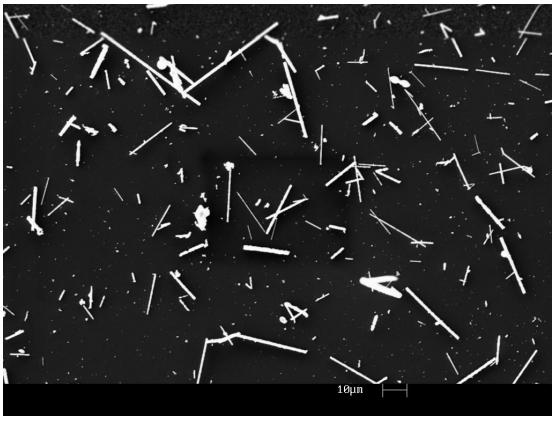

(j)

FIG. 9.—SEM images of dust samples consisting of irregularly shaped grains: (*e*) small diamond grains, (*f*) large diamond grains, (*g*) enstatite grains, (*h*) small silicon carbide grains, (*i*) large silicon carbide grains, and (*j*) silicon carbide whiskers. In contrast to Fig. 3, these images show samples dispersed by the cogwheel dust-jet generator.

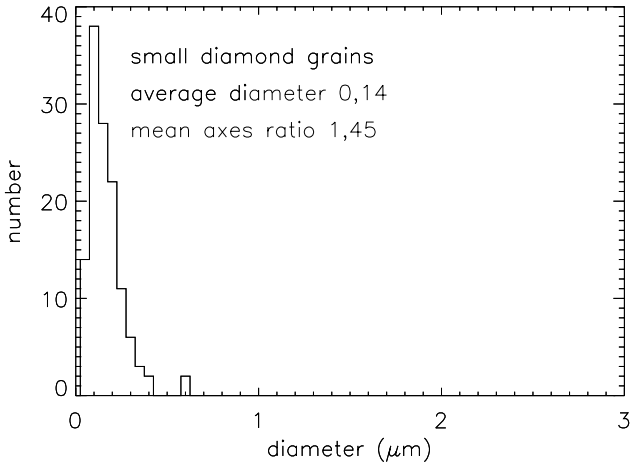

(e)

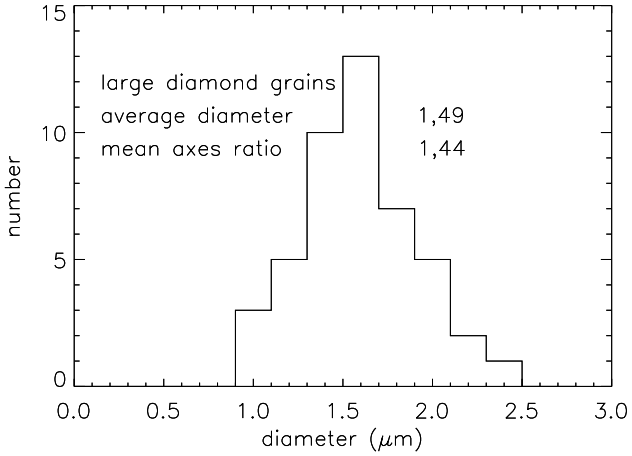

(f)

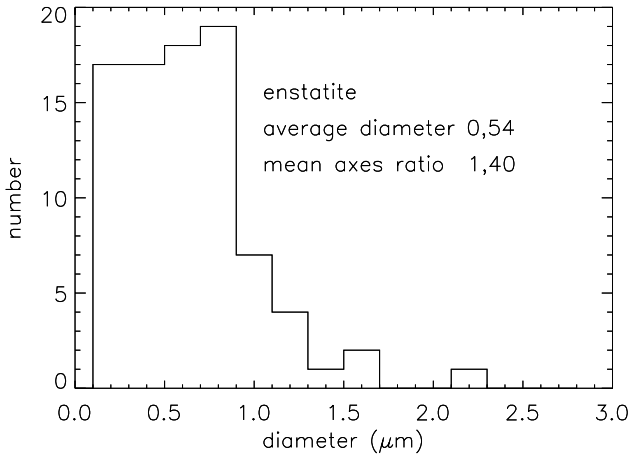

(g)

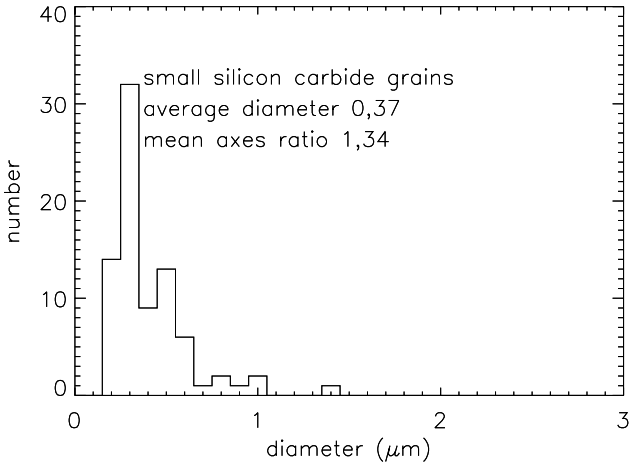

(h)

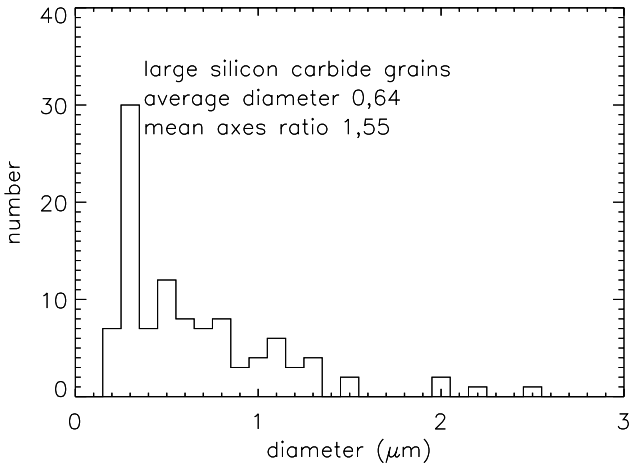

(i)

FIG. 10.—Size distributions of dust samples consisting of irregularly shaped grains: (*e*) small diamond grains, (*f*) large diamond grains, (*g*) enstatite grains, (*h*) small silicon carbide grains, and (*i*) large silicon carbide grains. The size is the mean of the long and of the short axes presented in the two-dimensional images of Fig. 9.

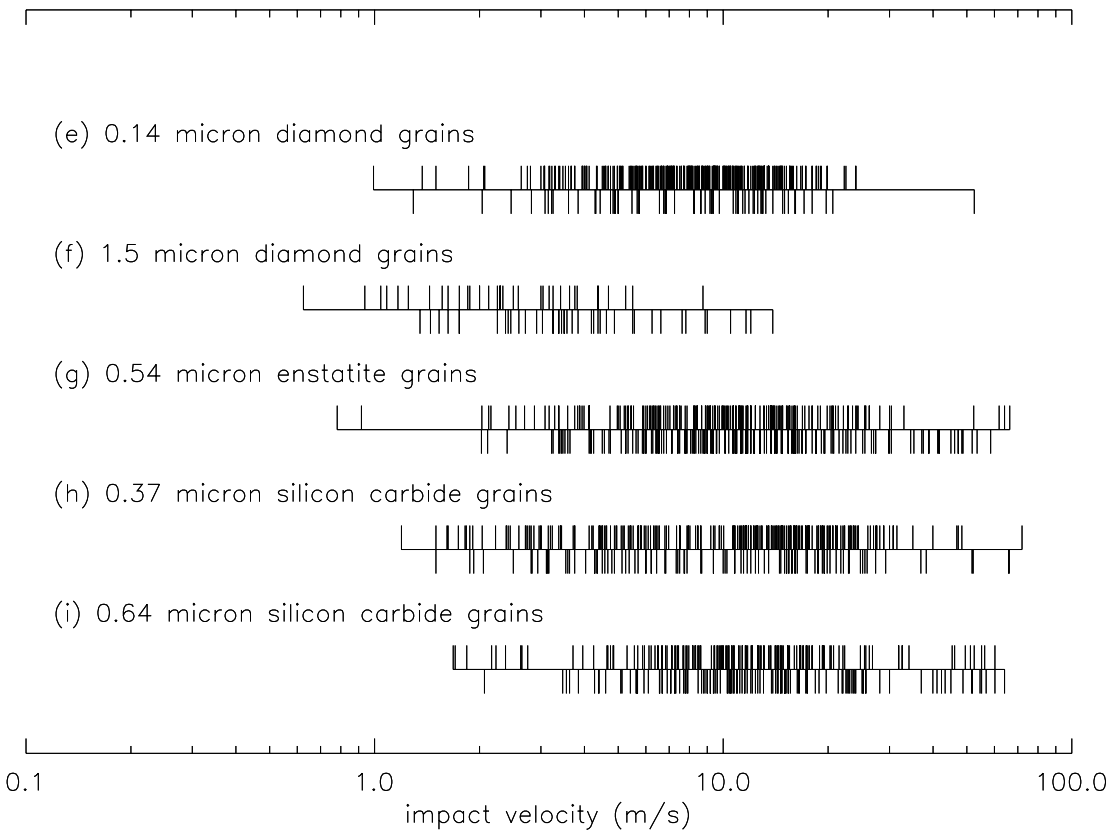

FIG. 11.—Dust sample and impact velocity for all collisions of the irregularly shaped grains with a silica target. A tick to the top indicates sticking; a tick to the bottom, bouncing.

grains than for spherical grains of comparable size. This can be seen, for example, by comparison of the sample of large silica spheres with the sample of large diamond grains. The comparison of the sample of large SiC grains, enstatite grains, and sample of small silica spheres, which all have a similar average diameter, shows that the increase in sticking probability owing to irregular shape is even stronger for the submicron-sized grains than for the larger ones. A hypothesis that can account for an increase in sticking probability and the lack of a well-defined capture velocity is that irregularly shaped particles often undergo multiple contacts with the impacted surface after the first contact. By the rebound at the point of first contact, which, in general, has not been beneath the center of mass, the particles acquire additional angular momentum and may then rotate in a way that favors a second contact between particle and substrate. The particles undergo this next contact with reduced impact velocity that may then more easily result in sticking than the first collision. A further description of this effect is given in the Appendix using a simple two-dimensional model. Possibly, even more than two surface contacts occur. This effect can cause sticking also for the several 10 μm long silicon carbide whiskers impacting with ≈ 10 m s^{-1}. The kinetic energy dissipation due to multiple contacts is especially effective if low coefficients of restitution are typical for a single contact. It is likely that the coefficient of restitution

TABLE 3

CAPTURE VELOCITY AND STICKING PROBABILITY OF ALL COMBINATIONS OF DUST SAMPLES AND TARGETS

Panel[a]	Average Diameter (μm)	Diameter Range (μm)	Dust Sample	Target	Capture Velocity (m s^{-1})	Sticking Probability	Velocity Range (m s^{-1})
a.....	1.2	...	Silica spheres	Polished silica	1.1–1.3	...	...
b.....	1.2	...	Silica spheres	Silicon wafer	1.1–1.3	...	...
c.....	0.5	...	Silica spheres	Polished silica	...	0.13	0.5.–18
d.....	0.5	...	Silica spheres	Silicon wafer	1.5–2.3	...	...
e.....	0.14	0.1–0.4	Diamond grains	Polished silica	...	0.79	1–23
f	1.5	1.3–1.9	Diamond grains	Polished silica	2.3–3.2	...	...
g.....	0.54	0.2–1.0	Enstatite grains	Polished silica	5–25	0.51	1–65
h.....	0.37	0.2–0.6	SiC grains	Polished silica	...	0.70	1.3–75
i	0.64	0.2–0.9	SiC grains	Polished silica	3.2–53	0.56	1.8–70
j	10–90	10–90	SiC whiskers	Polished silica	...	0.08	1–22

[a] The letters in the first column correspond to those in Figs. 6 and 12.

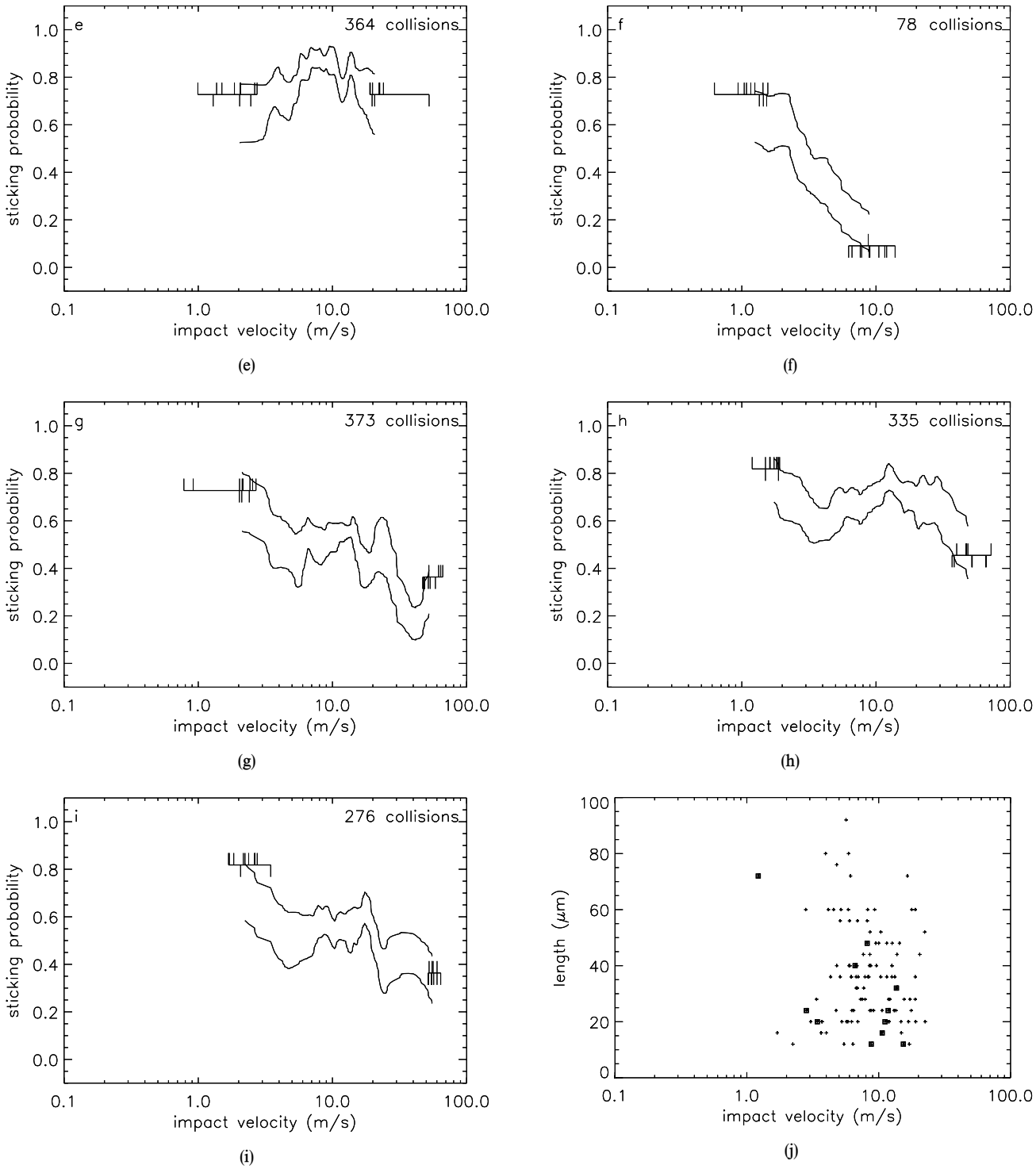

FIG. 12.—Sticking probability as a function of impact velocity for the irregular grains impacting polished silica: (*e*) diamond grains of average diameter 0.14 μm, (*f*) diamond grains of average diameter 1.5 μm, (*g*) enstatite grains of average diameter 0.54 μm, (*h*) silicon carbide grains of average diameter 0.37 μm, (*i*) silicon carbide grains of average diameter 0.64 μm, and (*j*) silicon carbide whiskers. The upper and lower 1 σ limits are shown. Additionally for the slowest and fastest collisions, the average values of the sticking probability are shown as a constant value with each single collision marked in the way introduced in Fig. 11. On the lower right, the sticking (*square*) or bouncing (*cross*) of the silicon carbide whiskers is shown indicating the impact velocity and the length of the whisker.

for a single contact is, in fact, low because this was found with the silica spheres as presented in § 3. The spherical grains lost the majority of their translational energy. For impact velocities exceeding 10 m s^{-1}, the kinetic energy is even reduced by 1 order of magnitude during the first contact. With the irregular grains, e was normally too small to be determined. This means that in most collisions, the quantity e was smaller than 0.1. This supports the hypothesis that the particles typically undergo more than one contact with the surface and each contact reduces the kinetic energy of the particle.

Compared to the important influence of particle mor-

phology on the collisional behavior, the influence of material is relatively unimportant among the materials used in our experiments. This is particularly obvious if one compares the enstatite dust sample to the large silicon carbide dust sample, both of which have a similar size distribution (see Fig. 10) and a similar sticking probability (see Fig. 12). Additionally, sticking collisions of the silicon carbide whiskers were more often observed for short whiskers than for long ones. On the other hand, there is no obvious influence of impact velocity on the sticking probability since there is no velocity interval in which sticking collisions were more often observed than in others. This emphasizes that grain size and shape are the main factors in determining the outcome of a collision.

5. SUMMARY AND CONCLUSION

We presented collision experiments with micron-sized silica spheres impacting silica and silicon targets. The dust grains had, owing to their sizes in the micron and submicron range and their hardnesses, the smallest contact radii ever investigated in particle collision experiments. For the first time, sticking of micron-sized grains was directly observed instead of being concluded from measurements of the coefficient of restitution or from the effectiveness of an aerosol filtration process. We presented collisions with impact angles between 0° (normal impact) and 60°. We found that the collisional behavior of spheres can generally be described by a capture velocity as done by previous researchers, both theoretical and experimental. The capture velocity is typically a few meters per second for micron size, which is very similar to former experiments of Dahneke (1975) with almost equally sized spheres. However, the capture limit is more than 1 order of magnitude higher than predictions by the model of Chokshi et al. (1993). We excluded that this is due to increased surface energies or due to the plastic deformation of tiny surface roughnesses. In consequence, this must be caused by an effective and hitherto underestimated dissipation of energy in the bulk material. For the first time, we investigated the sticking probability of irregularly shaped grains, and we found that the sticking probability cannot easily be described by a capture velocity. Rather, the sticking probability is often close to neither 0 nor 1. The sticking probability is considerably increased for irregularly shaped particles as compared to spherical grains. When existing, the capture velocity is many times higher than the capture threshold for equally sized spheres. In all other cases, the collision process is well described by a constant or slightly decreasing sticking probability with increasing impact velocity. Many submicron-sized grains stick even at collision velocities exceeding 50 m s^{-1}. Silicon carbide whiskers with up to 50 μm length can stick at collision velocities around 10 m s^{-1}. This means that the restriction to spheres of former work on dust aggregation (Chokshi et al. 1993; Dominik & Tielens 1995 and 1997) is inadequate because irregularly shaped grains have a higher sticking probability and there is no doubt that such grains play an important role in the preplanetary dust aggregation (§ 1.2). Particle shape, size, and roughness are important for the sticking probability whereas the particle material is unimportant among the materials used here (silica, enstatite, diamond, and silicon carbide).

We conclude that the preplanetary dust aggregation is more effective than previously thought owing to a generally high sticking probability. According to Weidenschilling & Cuzzi (1993), the relative velocities between grains embedded in the solar nebula is determined by their sizes. In the context of this model, this means for 1 AU solar distance that micron-sized grains always stick to objects up to centimeter to decimeter size and can stick to objects of decimeter to meter size owing to effects of irregular grain shape.

In a separate paper (Poppe et al. 2000), we present experiments on the collisional electrostatic charging upon impact, which also contributes to the sticking probability in the sense that particles charged in a mechanically bouncing collision can attract each other and can thus finally stick.

We thank L. Heim for measuring the surface roughnesses presented in Table 1. We also thank the Deutsche Forschungsgemeinschaft (DFG), the Deutsches Zentrum für Luft- und Raumfahrt (DLR), and the Alfried Krupp von Bohlen und Halbach-Stiftung for funding of the work presented.

APPENDIX

Upon impact onto a flat target, irregularly shaped particles can undergo more than one contact with the surface, which can lead to an increased sticking probability and to the observed lack of a well-defined capture velocity. Although a detailed analysis of this shape effect is far beyond our experimental scope, we can explain some characteristics of this shape effect by a simple two-dimensional model.

With the object on the left in Figure 13, we model the irregular particle by two identical rings with radius r each carrying one half of the particle's mass. The rings are connected with their centers separated from the common center of mass by the distances s. Each ring has the moment of inertia $(1/2) \times (mr^2)$ around its center. The moment of inertia Θ of both rings around the center of mass is

$$\Theta = m(r^2 + s^2) . \tag{4}$$

We assume that the object vertically impacts the target with no initial rotation and with a small angle α between the target surface and the line connecting the two centers of the rings [$\cos(\alpha) \approx 1$; this is no serious restriction of generality since a realistic irregular object has many outstanding parts instead of only two in the model, thus allowing multiple contacts in many rotational positions]. We also assume that each contact with the surface can be described by a coefficient of restitution $e(v_i)$. The impact velocity at the first point of contact is

$$v_{1i} = v_i . \tag{5}$$

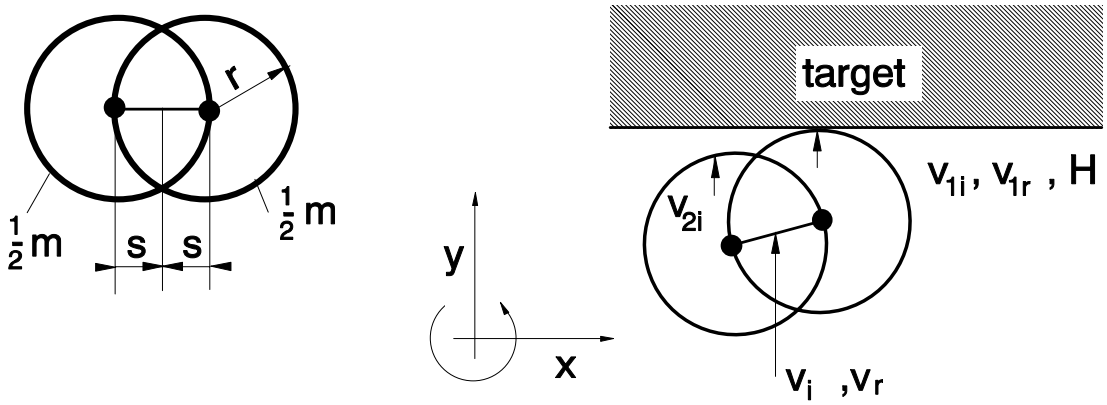

FIG. 13.—*Left-hand panel*: Two-dimensional model object to investigate effects of irregular grain shape. *Center panel*: Model coordinates. *Right-hand panel*: Model object impacts the target at the first point of contact.

After the first contact, ω_r is the angular velocity around the center of mass and v_r its translational velocity. Thus the rebound velocity at the first point of contact is

$$v_{1r} = v_r + s\omega_r \,. \tag{6}$$

With the coefficient of restitution $e(v_{1i})$, we can write

$$v_{1r} = -ev_{1i} \,. \tag{7}$$

The impact velocity at the second point of contact is

$$v_{2i} = v_r - s\omega_r \,. \tag{8}$$

Conservation of momentum requires

$$mv_i = mv_r + H \,, \tag{9}$$

in which H is the momentum transferred to the target. After the first contact, the angular momentum around the center of mass is

$$0 = m(s^2 + r^2)\omega_r + sH \,. \tag{10}$$

Using equations (9) und (10), we obtain

$$v_r = \frac{s^2 + r^2}{s}\,\omega_r + v_i \,. \tag{11}$$

With equations (5), (6), and (7), we can write

$$v_r = -ev_i - s\omega_r \,. \tag{12}$$

Equating equations (11) and (12) yields

$$\omega_r = -(1 + e)\,\frac{s}{2s^2 + r^2}\,v_i \,. \tag{13}$$

Inserting equation (13) into equation (11) results in

$$v_r = \left[1 - (1 + e)\,\frac{s^2 + r^2}{2s^2 + r^2}\right]v_i \,. \tag{14}$$

With equations (13) and (14) used in equation (8), we obtain

$$v_{2i} = \left[1 - (1 + e)\,\frac{r^2}{2s^2 + r^2}\right]v_i \,. \tag{15}$$

If v_{2i} has the same sign as v_i (here: positive) there will be a second contact at a second point. If v_{2i} is less than the capture velocity the second contact will result in sticking. Equation 15 shows that a second contact is favored by a small e and a large s. On the other hand, the impact velocity at the second point of contact v_{2i} will be large, thus favoring rebound, if s is large. This indicates a complex sticking behavior not necessarily marked by one single capture velocity but possibly by intervals that favor sticking or bouncing, as we will see below.

As an example, an irregular model object was chosen representing properties of the small silica spheres. The ring radius is $r = 0.25$ μm, and two functions $e(v_i)$ were generated shown in Figure 14 (*left*) that have values of e comparable to the values

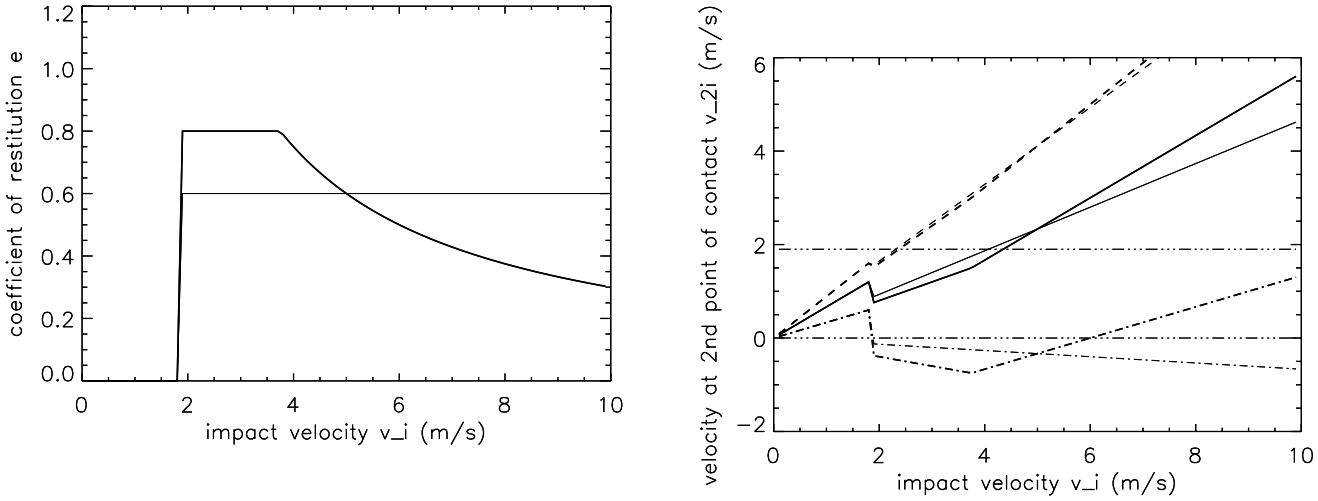

FIG. 14.—*Left-hand panel*: Two arbitrarily generated functions $e(v_i)$ on which the diagram on the right is based. *Right-hand panel*: Velocity v_{2i} at the second point of contact as a function of v_i for different values of s. The solid lines denote $s = r$, the dashed lines $s = 2r$, and the dashed-dotted lines $s = r/2$. The thick and the thin lines are based on the corresponding lines in the diagram on the left. Sticking will occur if v_{2i} is smaller than v_c and larger than 0. This interval is marked by the thin lines parallel to the abscissa.

shown in Figure 8 and with $e = 0$ for $v_i \leq 1.9$ m s^{-1}. For three different values of s, representing different shapes, the collision velocity at the second point of contact v_{2i} can be calculated according to equation (15) and is shown in Figure 14 (*right*).

The impact velocity at the second point of contact is always smaller than at the first point; thus, a second contact favors sticking. Furthermore, there is a combination of s, r, and $e(v)$, which has not only one capture velocity but two intervals of sticking and bouncing.

We thus find that an increased sticking probability and the lack of a capture velocity can be explained by an effect of irregular grain shape. In reality, the grains and the collisional conditions are not uniform but statistically distributed in size, rotation, and shape of the grains, which could lead to a velocity-dependent sticking probability that is often neither close to 0 nor to unity as found for most irregular grains.

REFERENCES

Anders, E., & Zinner, E. 1993, Meteoritics, 28, 490
Artymowicz, P. 1994, in Circumstellar Dust Disks and Planet Formation, ed. R. Ferlet & A. Vidal-Madjar (Gif-sur-Yvette: Editions Frontières), 47
Beckwith, S. V., Henning, Th., & Nakagawa, J. 1999, in Protostars and Planets IV, ed. V. Mannings, A. Boss, & S. Russell (Tucson: Univ. of Arizona Press), in press
Broom, G. P. 1979, Filtration and Separation, November/December, 661
Cheng, Y., & Yeh, H. 1979, Environ. Sci. Technol., 13, 1392
Chokshi, A., Tielens, A. G. G. M., & Hollenbach, D. 1993, ApJ, 407,806
Dahneke, B. E. 1971, J. Colloid Interface Sci., 37, 342
———. 1975, J. Colloid Interface Sci., 51, 58
———. 1995, Aerosol Sci. Technol., 23, 25
Dominik, C., & Tielens, A. G. G. M. 1995, Philos. Mag. A, 72(3), 783
———. 1997, ApJ, 480, 647
Dorschner, J., Begemann, B., Henning, Th., Jäger, C., & Mutschke, H. 1995, A&A, 300, 503
D'Ottavio, T., & Goren, L. 1983, Aerosol Sci. Technol., 2, 91
Esmen, N. A., Ziegler, P., & Whitfield, R. 1978, J. Aerosol Sci., 9, 547
Gail, H.-P. 1998, A&A, 322, 1099
Grossman, L., & Larimer, J. W. 1974, Rev. Geophys. Space Phys., 12(1), 71
Grün, E., Gustafson, B., Mann, I., Baguhl, M., Morfill, G. E., Staubach, P., Taylor, A., & Zook, H. A. 1994, A&A, 286, 915
Heim, L.-O., Blum, J., Preuss, M., & Butt, H.-J. 1999, Phys. Rev. Lett., 83(16), 3328
Hertz, H. 1882, J. Reine Angew. Math., 92, 155
John, W. 1995, Aerosol Sci. Technol., 23, 1
Johnson, K. L., Kendall, K., & Roberts, A. D. 1971, Proc. R. Soc. London A, 324, 301
Kendall, K., Alford, N. M., & Birchall, J. D. 1987, Nature, 325, 794
Kerridge, J. F. 1993, Icarus, 106, 135
Kerridge, J. F., & Chang, S. 1987, in Protostars and Planets II, ed. D. C. Black & M. S. Matthews (Tucson: Univ. of Arizona Press), 738
Kim, S. H., Martin, P. G., & Hendry, P. D. 1994, ApJ, 422, 164
Mathis, J. S., Rumpl, W., & Nordsieck, K. H. 1977, ApJ, 217, 425
Nuth, J. A., Berg, O., Faris, J., & Wasilewski, P. 1994, Icarus, 107, 155
Pollack, J. B., Hollenbach, D., Beckwith, S., Simonelli, D. P., Roush, T., & Fong, W. 1994, ApJ, 421, 615
Poppe, T. 1998, Ph.D. thesis, Friedrich-Schiller-Universität, Jena
Poppe, T., & Blum, J. 1997, Adv. Space Res., 20(8), 1595
Poppe, T., Blum, J., & Henning, Th. 1997, Rev. Sci. Instrum., 68(6), 2529
———. 2000, ApJ, in press
Rogers, L. N., & Reed, J. 1984, J. Phys. D., 17, 677
Tsai, C. J., Pui, D. Y. H., & Liu, B. Y. H. 1990, Aerosol Sci. Technol., 12, 497
Wall, S., John, W., Wang, H., & Goren, S. L. 1990, in Aerosol Sci. Technol., 12, 926
Wang, H., & John, W. 1988, in Particles on Surfaces 1, Dynamic Adhesion of Particles Impacting a Cylinder, ed. K. L. Mittal (New York: Plenum), 211
Weidenschilling, S. J., & Cuzzi, J. N. 1993, in Protostars and Planets III, ed. E. Levy, J. Lunine, & M. S. Matthews (Tucson: Univ. of Arizona Press), 1031